electronic reprint

Journal of
Applied Crystallography
ISSN 0021-8898

Rietveld refinements on laboratory energy dispersive X-ray diffraction (EDXD) data

Paolo Ballirano and Ruggero Caminiti

Journal of
Applied Crystallography
ISSN 0021-8898

Received 23 April 2001
Accepted 7 September 2001

Rietveld refinements on laboratory energy dispersive X-ray diffraction (EDXD) data

Paolo Ballirano[a]* and Ruggero Caminiti[b]

[a]Dipartimento di Scienze della Terra, Università di Roma "La Sapienza", P. le Aldo Moro 5, I-00185 Roma, Italy, and [b]Dipartimento di Chimica, Istituto Nazionale per la Fisica della Materia, Università di Roma "La Sapienza", P. le Aldo Moro 5, I-00185 Roma, Italy. Correspondence e-mail: paolo.ballirano@uniroma1.it

Rietveld refinements of corundum, a rutile and anatase nanocrystalline synthetic mixture, and gypsum, on laboratory energy dispersive X-ray diffraction (EDXD) data are reported. Cell parameters, positional and displacement parameters are in reasonable agreement with single-crystal reference data, despite the rather poor resolution of EDXD data. In particular, good results were obtained for gypsum (unrestrained refinement) with counting times as short as 1000 s.

1. Introduction

The original development of a laboratory energy dispersive system to analyse a crystalline specimen was carried out in the late 1960s (Giessen & Gordon, 1968). In this technique, the unfiltered radiation from a commercial X-ray source impinges on a specimen and the diffracted beam is energy-resolved by a solid-state detector located at a suitable scattering angle. The modulus of the scattering vector q (function of the energy of the photon E and the scattering angle θ) can be represented as

$$q(E,\theta) = 1.01354E\sin\theta = 4\pi(\sin\theta)/\lambda, \qquad (1)$$

where q is expressed in Å^{-1}, λ in Å, and E in keV.

Some subsequent applications of the energy dispersive X-ray diffraction (EDXD) powder method on laboratory instruments have been reported (*e.g.* Drever & Fitzgerald, 1970; Ferrel, 1971; Laine *et al.*, 1974; Nakajima *et al.*, 1976; Nuding *et al.*, 1980; Eisenreich & Engel, 1983; Uno & Ishigaki, 1984). The rather poor intrinsic resolution of the EDXD system has severely limited its application in structural analysis. In fact, the relative resolution of an EDXD system is largely dominated by the contribution from the detector (Otto, 1997),

$$\frac{\Delta E_{\rm FWHM}}{E} = \left\{\frac{\Delta E_{\rm amp}^2}{E^2} + \left[(2.354)^2\frac{F\varepsilon}{E}\right] + (\cot\theta_0\Delta\theta)^2\right\}^{1/2} \qquad (2)$$

where $\Delta E_{\rm FWHM}$ represents the full width at half-maximum (FWHM) at energy E, $\Delta E_{\rm amp}$ is the energy resolution of the electronic circuit, F is the Fano factor, and ε is the energy required to create an electron–hole pair. The last term is the simplified expression, obtained from differentiation of Bragg's law, for equatorial beam divergence $\Delta\theta$ at the diffraction angle θ_0. Despite this limitation, a few quantitative structural studies by means of EDXD on synchrotron sources have been carried out (Glazer *et al.*, 1978; Buras *et al.*, 1979; Yamanaka & Ogata, 1991). The method has gained increasing popularity as a tool to monitor the change of lattice parameters with pressure (P) and/or temperature (T) in order to derive the corresponding equation of state (see for example Grevel *et al.*, 2000) or to detect the occurrence of phase transformations (Zhang & Guyot, 1999). Both whole-pattern powder decomposition (Morishima *et al.*, 1999) and Rietveld refinement (Frost & Fei, 1999) have been carried out on EDXD data, but apparently to determine cell parameters only. Only recently has this technique been re-addressed toward laboratory instruments. In fact, in spite of the lack of resolution, EDXD has proved to be especially suited for structural studies of low-crystallinity, amorphous, or liquid materials (Rossi Albertini, Bencivenni *et al.*, 1996; Rossi Albertini, Caminiti *et al.*, 1997; Sugiyama *et al.*, 1998), as well as for the study of the kinetics of phase transitions (Ballirano *et al.*, 1998; Caminiti & Rossi Albertini, 1999).

The aim of this paper is to investigate the possibility to perform, *via* Rietveld refinement, reliable structure analyses using laboratory EDXD data on fully crystalline samples. This opportunity seems particularly attractive in order to follow structural behaviours during phase transitions, at least in the case of simple structures. In order to test the possibility we have collected powder data on SRM676 α-Al_2O_3, a 20/80 wt% nanocrystalline rutile/anatase (TiO_2 polymorphs) synthetic mixture, and gypsum $CaSO_4.2H_2O$. These materials were selected because they show different degrees of structural complexity and very different tendencies to be affected by preferred orientation.

2. Experimental

Powder X-ray data were collected with a prototype EDXD instrument (Caminiti, Sadun *et al.*, 1991; Caminiti, Sadun, Bionducci *et al.*, 1997) characterized by vertical θ/θ geometry (see Fig. 1 of Caminiti *et al.*, 1999). It consists of a commercial Seifert X-ray generator (W target), a collimating system, step motors, and a solid-state detector (SSD) linked *via* an electronic circuit to a multichannel analyser (MCA). A thermo-

static cell can be optionally placed at the common centre of rotation of the diffractometer arms (Rossi Albertini, Caminiti *et al.*, 1997). The detecting system is composed of an EG&G liquid-nitrogen-cooled ultrapure Ge SSD ORTEC 92X connected to a PC through ADCAM hardware. The collimating system is composed of four adjustable (both vertically and axially) W slits, two of which are fitted along the incident beam (post Be window and divergence) and two along the diffracted beam (antidivergence and receiving). No Soller slits were inserted along the optical path. Step motors were used to rotate both the X-ray tube and the detector holding arms around their common centre up to the desired scattering angle (reproducibility $>0.001^\circ$ 2θ). The sample can be fitted either in reflection or in transmission mode. The powdered samples were pressed in order to obtain pellets of 12 mm diameter and with a thickness of *ca* 1 mm. Data were collected in symmetrical transmission mode (Wilson, 1973) as this configuration is particularly convenient because all optical paths through the sample have the same length regardless of the depth of the scattering point from the surface. In this case, the coherent absorption can be simply expressed as

$$A_{\rm coh}(E,\theta) = \exp[-\mu(E)t\sec\theta]. \quad (3)$$

Calibration of the scattering angles was carried out using National Institute of Standards and Technology (NIST) Standard Reference Material (SRM) 640b Si. MCA calibration was performed using the absorption edges of Zr, Ru, Pd, Ag, In, I, Ce, Gd and Dy. Linearity between channel number and energy was confirmed by a regression coefficient R^2 of 1. Dead time was kept to <2% throughout the measurements. Different opening apertures of the slits were used for the three samples in order to maximize the intensity without significant loss of resolution. The post Be-window slit was kept fixed to the values of 500 (height) × 8000 (width) μm. The aperture dimensions are significantly larger than those reported in synchrotron measurements, where beam diameters of *ca* 50 μm are commonly used (Yamanaka & Ogata, 1991), but this is an obvious consequence of the very different source brightness.

3. Data evaluation

3.1. SRM676 α-Al_2O_3

The standard procedure of data evaluation will be described in detail for SRM676 α-Al_2O_3. For the other substances, only different strategies, whenever adopted, will be reported.

A scattering angle θ of 15.63° was selected. Of the 1024 channels of the MCA, a total of 465 data points were evaluated. This is because the first 184 channels were not used as they contain the fluorescence L lines of W (8–11 keV range), and the last 375 channels because the counting statistics were considered inadequate. This data set covers the range $0.53 < d_{hkl} < 1.83$ Å. The X-ray source operated at 45 kV and 40 mA. A counting time of 42500 s was used. Slit apertures were 300 × 3000, 300 × 3000, and 600 × 3000 μm. Raw data were normalized to the incident white spectrum (fitted with a sixth-order polynomial), corrected for absorption and escape peaks, and subsequently interpolated to obtain constant-q data using laboratory software. Interpolation did not introduce any extra data points. The calculation of the experimental

$$\exp[-\mu(E)t] = I_t(E)/I_0(E), \quad (4)$$

to be used in (3) for absorption correction, was carried out by measuring the intensity of the transmitted beam through the sample, $I_t(E)$, and of the incident primary beam, $I_0(E)$, both collected in direct transmission ($\theta = 0^\circ$) at 45 kV and 5 mA (Fig. 1). Escape peak correction was carried out using a calibration curve that was built-up by evaluation of the dependency of escape efficiency *versus* energy by measurement of *hhh* reflections from a Si single-crystal plate.

Diffraction data were evaluated by the *GSAS* crystallographic package (Larson & Von Dreele, 1985). This suite of programs is, in fact, able to handle constant-q data by conversion to conventional ADXD data using a fictitious user-defined wavelength (Mo $K\alpha_1$ = 0.70926 Å throughout this work). Preliminary single-peak profile fitting indicated that a simple Gaussian function was adequate to fit the data owing to the low resolution of the instrumental setup. Peak shape was therefore initially modelled by means of a standard Gaussian function modified for peak asymmetry (Rietveld, 1969). A significant improvement of the fit was subsequently obtained using a pseudo-Voigt function (Thompson *et al.*, 1987), modified to incorporate asymmetry (Finger *et al.*, 1994). The *LX* and *LY* Lorentzian parameters refined to zero, in accord with the expectation that small size and strain broadening effects are not detectable at this level of resolution. Refined parameters included: $\tan^2\theta$-dependent, $\tan\theta$-dependent and θ-independent (*GU*, *GV* and *GW*, respectively) Gaussian parameters, and the asymmetry parameters S/L and H/L (constrained to be equal). The better behaviour of this function with respect to the standard Gaussian function arises from the more sophisticated asymmetry modelling. The peak cut-off was set to 0.01% of the peak maximum. The background was

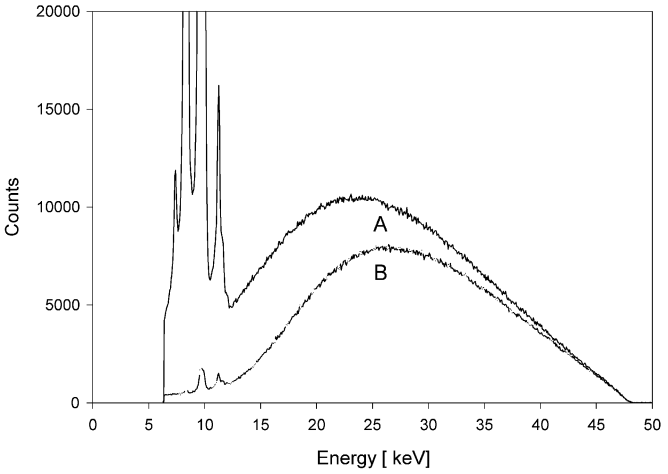

Figure 1
Incident white beam (A) and transmitted beam (B) measured at $\theta = 0^\circ$ (direct transmission) for the synthetic mixture of rutile and anatase.

Table 1
Miscellaneous data for the refinement of SRM676 α-Al_2O_3.

Statistical indicators are defined according to Young (1993). Selected reference data on α-Al_2O_3 are reported for comparison: (*a*) Oetzel & Heger (1999); (*b*) Cline & Cheary (1998); (*c*) Thompson *et al.* (1987); (*d*) Hill & Madsen (1986); (*e*) Will *et al.* (1983); (*f*) Lewis *et al.* (1982).

	This work	(*a*)	(*b*)	(*c*)	(*d*)	(*e*)	(*f*)
Data collection	EDXD	ADXD	ADXD	ADXD	ADXD	ADXD	Single crystal
Source	W target	Cu target	Cu target	Synchrotron	Cu target	Cu target	Mo target
Data evaluation	Rietveld	Rietveld	Rietveld	Rietveld	Rietveld	Profile fitting	–
Experimental points	465	14001	13397	7501	10480	–	397†
R_p (%)	2.00	8.41	8.30	–	6.65	–	–
wR_p (%)	2.82	12.2	11.32	22.2	8.69	–	–
R_B (%)	3.07	3.62	3.32	6.6	4.01	1.4	1.5‡
DWd	0.583	2.364	0.388	–	0.069	–	-
Refined parameters	26	20	18	10	14	–	44
Reduced χ^2	3.161	1.49	6.27	2.38	14.72	–	2.90
J	1.013	–	–	–	–	–	–
a (Å)	4.7599 (5)	4.7589 (1)	4.75925 (1)	4.7586 (1)	4.75980 (2)	–	4.7602 (4)
c (Å)	12.994 (2)	12.991 (1)	12.99191 (4)	12.9897 (1)	12.9936 (1)	–	12.993 (2)
z_{Al}	0.35241 (8)	0.35222 (4)	0.35220 (2)	0.3518 (1)	0.35211 (3)	0.3523 (1)	0.35216 (1)
x_O	0.3063 (4)	0.3066 (2)	0.3062 (1)	0.3082 (6)	0.3064 (1)	0.3057 (5)	0.30624 (4)
B_{iso} Al	0.50 (2)	0.26 (2)	0.197 (5)	0.68 (5)	0.381 (8)	0.75 (8)	0.225 (2)§
B_{iso} O	0.40 (3)	0.14 (2)	0.11 (1)	0.71 (7)	0.52 (2)	1.09 (7)	0.272 (2)§

† Unique reflections. ‡ $wR(|F|^2)$. § Recalculated from anisotropic displacement parameters.

fitted with an eight-term Chebyshev polynomial of the first kind. A zero-correction for detector position was also refined. The presence of texture was checked, during the last cycle of refinement, by means of a generalized spherical-harmonic description (Von Dreele, 1997). Six terms up to the sixth order were introduced, but resulted in no significant improvement of the fit because the texture index, *J*, was 1.013. The total number of refined parameters was 26. Miscellaneous data of the refinement are reported in Table 1; experimental, calculated and difference plots are presented in Fig. 2.

3.2. Synthetic mixture of nanocrystalline rutile and anatase

A sample of P 25 S (Degussa-Hüls) was also investigated. This material is composed of a nanocrystalline (average dimension of 210 Å) mixture of rutile (*ca* 20 wt%) and anatase (*ca* 80 wt%), two tetragonal TiO_2 polymorphs. A scattering angle θ of 11.13° was chosen. A total of 525 data points, covering the $0.60 < d_{hkl} < 2.68$ Å range, were evaluated. A counting time of 41500 s was used. The X-ray source operated at 50 kV and 40 mA. Slit apertures were 200 × 3000, 200 × 3000, and 400 × 3000 µm. Miscellaneous data of the refinement are reported in Table 2; experimental, calculated and difference plots are presented in Fig. 3.

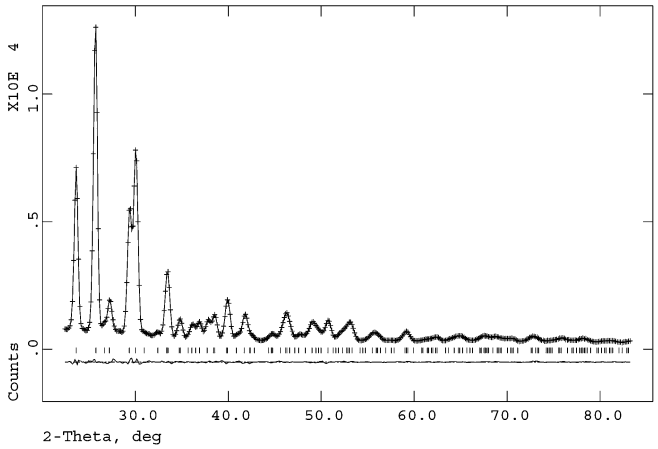

Figure 2
Experimental (dots) and calculated (continuous line) patterns of SRM676. The difference profile is shown at the bottom of the figure. Vertical markers refer to the positions of the calculated Bragg reflections.

The structure of rutile was kept fixed to the reported parameters of Shintani *et al.* (1975). Peak shape was constrained to be equal for the two phases. The presence of texture was checked for anatase only (five terms up to the sixth order). The refined *J* index was found to be very close to one.

3.3. $CaSO_4.2H_2O$

A scattering angle θ of 12.15° was selected. Following the procedure described for α-Al_2O_3, 493 data points were evaluated, covering the $0.65 < d_{hkl} < 2.31$ Å range. The X-ray source operated at 48 kV and 40 mA. Slit apertures were 300 × 4000, 300 × 4000, and 600 × 4000 µm. Several scans were collected using different counting times, ranging from 1000 to 20000 s. Auxiliary scans were carried out, varying the slit dimensions in order to investigate the effect on peak variance and asymmetry. The FWHM value was found to vary from 0.68 to 0.93° at 20° 2θ of Mo passing from 100 to 400 µm of vertical aperture. This dependence has been empirically approximated in this aperture interval by the following polynomial (R^2 = 0.99999):

$$\mathrm{FWHM} = 0.72025 - 7.335 \times 10^{-4} \times (\mathrm{width}) + 3.125 \times 10^{-6} \times (\mathrm{width})^2. \quad (5)$$

The background was fitted with a 13-term Chebyshev polynomial of the first kind. No restraints were imposed on bond angles and distances. The presence of preferred orientation was detected and modelled by spherical harmonics (eight

Table 2
Miscellaneous data for the refinements of the rutile and anatase mixture.

Statistical indicators are defined according to Young (1993). Selected reference data on rutile and anatase are reported for comparison: (*a*) Shintani (1975); (*b*) Horn *et al.* (1972).

	This work	(*a*)	(*b*)
Data collection	EDXD	Single crystal	Single crystal
Source	W target	Mo target	Mo target
Data evaluation	Rietveld	–	–
Experimental points	525	302†	–
R_p (%)	3.16	–	–
wR_p (%)	4.29	–	–
DWd	0.643	–	–
Refined parameters	49	–	–
Reduced χ^2	2.680	–	–
J_{ana}	1.020	–	–
a_{rut} (Å)	4.593 (2)	4.5845 (1)	–
c_{rut} (Å)	2.961 (1)	2.9533 (1)	–
a_{ana} (Å)	3.7840 (7)	–	3.784 (1)
c_{ana} (Å)	9.500 (2)	–	9.515 (1)
x_{rut} O	0.30493 (0)	0.30493 (7)	–
B_{iso} Ti	0.50 (0)	0.499 (4)‡	–
B_{iso} O	0.56 (0)	0.56 (1)‡	–
z_{ana} O	0.3339 (6)	–	0.3331 (2)
B_{iso} Ti	0.50 (8)	–	0.39 (6)
B_{iso} O	0.7 (1)	–	0.61 (9)
wt% rutile	18.0 (4)	–	–
wt% anatase	82.0 (3)	–	–

† Unique reflections. ‡ Recalculated from anisotropic displacement parameters.

terms up to the fourth order), significantly improving the fit as a result of *J* indices of *ca* 1.8. The presence of texture agrees with the easy [010] cleavage shown by gypsum. Miscellaneous data of the refinements are reported in Table 3, with relevant bond distances and angles in Table 4; experimental, calculated and difference plots are presented in Fig. 4.

4. Discussion

As may be observed from Tables 1–4, the results of the structure refinements lead to positional and displacement parameters that are reasonably close to those reported in reference data, despite the low resolution of the EDXD data. In particular, in the case of Al_2O_3, deviations of the *z* coordinate of Al and the *x* coordinate of O from single-crystal values (Lewis *et al.*, 1982) were 3.5σ and 1σ, respectively. Standard deviations are of one order of magnitude greater than those of single-crystal data. They are, however, smaller than those reported by Glazer *et al.* (1978) for $BaTiO_3$ and by Yamanaka & Ogata (1991) for GeO_2 at room pressure. No direct comparison is possible with the results of Buras *et al.* (1979) on urea (restrained refinement) and naphthalene (rigid-body refinement). Isotropic displacement parameters are larger than those determined through single-crystal analysis but are within the range of those reported for powder data. In addition, the refined cell parameters of Al_2O_3 are of good quality, being within 2σ of the values of a = 4.75925 Å, c = 12.99191 Å (NIST SRM676 certificate).

Table 3
Miscellaneous data for the refinements of $CaSO_4.2H_2O$ carried out with different counting times, ranging from 1000 to 20000 s.

Statistical indicators are defined according to Young (1993). Selected reference data on $CaSO_4.2H_2O$ are reported for comparison: (*a*) Pedersen & Semmingsen (1982); (*b*) Cole & Lancucki (1974).

	This work	(*a*)	(*b*)
Data collection	EDXD	Single crystal	Single crystal
Source	W target	Neutron	Mo target
Data evaluation	Rietveld	–	–
Experimental points	493	611†	365†
R_p (%)	1.14–3.23	–	–
wR_p (%)	1.51–4.22	–	–
R_B (%)	2.49–3.32	4.3‡	7.4‡
DWd	0.657–1.770	–	–
Refined parameters	47	57	–
Reduced χ^2	1.260–6.452	1.28	–
J	1.839–1.896	–	-
a (Å)	5.681 (1)–5.686 (2)	5.679 (5)	5.670 (2)
b (Å)	15.218 (9)–15.231 (6)	15.20 (1)	15.201 (2)
c (Å)	6.528 (1)–6.535 (2)	6.522 (6)	6.533 (2)
β (°)	118.43 (2)–118.46 (1)	118.43 (4)	118.60 (4)

† Unique reflections. ‡ $wR(|F|^2)$.

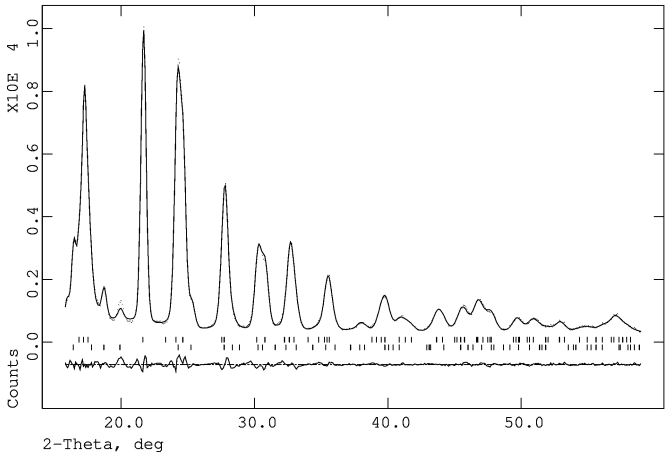

Figure 3
Experimental (dots) and calculated (continuous line) patterns of the synthetic mixture of rutile and anatase. Vertical markers: the first row refers to the positions of the calculated Bragg reflections for anatase; the second row indicates calculated Bragg reflections for rutile.

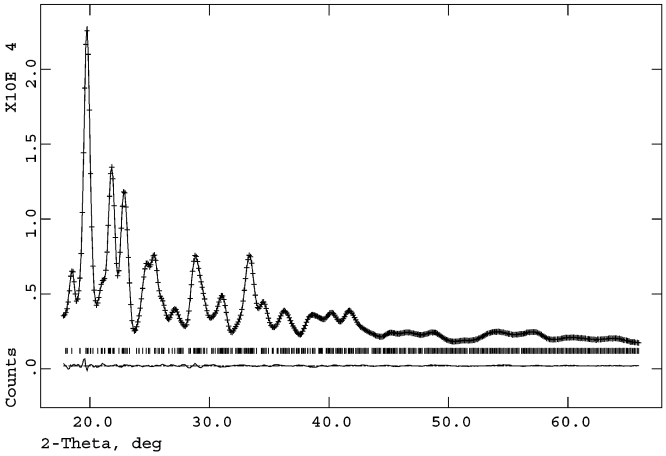

Figure 4
Experimental (dots) and calculated (continuous line) patterns of $CaSO_4.2H_2O$ from the data set with a counting time of 2000 s.

Table 4
Positional and displacement parameters and relevant bond distances and angles of $CaSO_4.2H_2O$ from data sets collected with different counting times.

Reference data sets: (*a*) Pedersen & Semmingsen (1982); (*b*) Cole & Lancucki (1974).

		x	*y*	*z*	B_{iso}
Ca	This work	$\frac{1}{2}$	0.0796 (2)–0.0803 (5)	$\frac{1}{4}$	1.2 (3)–1.3 (2)
	(*a*)	$\frac{1}{2}$	0.07967 (9)	$\frac{1}{4}$	1.754 (6)
	(*b*)	$\frac{1}{2}$	0.0797 (0)	$\frac{1}{4}$	0.51 (1)
S	This work	0	0.0778 (5)–0.0801 (10)	$\frac{3}{4}$	0.31 (6)–0.6 (2)
	(*a*)	0	0.0771 (1)	$\frac{3}{4}$	1.541 (8)
	(*b*)	0	0.0772 (0)	$\frac{3}{4}$	0.63 (1)
O1	This work	0.9644 (21)–0.9667 (10)	0.1329 (10)–0.1343 (6)	0.5530 (11)–0.5560 (10)	0.5 (2)–0.70 (8)
	(*a*)	0.9632 (1)	0.13190 (5)	0.5505 (1)	2.070 (3)
	(*b*)	0.9607 (3)	0.1312 (1)	0.5518 (2)	1.24 (2)
O2	This work	0.7560 (12)–0.7589 (22)	0.0219 (12)–0.0236 (6)	0.6604 (15)–0.6646 (20)	1.3 (4)–1.8 (2)
	(*a*)	0.7582 (1)	0.02226 (5)	0.6671 (1)	1.967 (3)
	(*b*)	0.7592 (2)	0.0227 (1)	0.6661 (2)	1.18 (2)
O*W*	This work	0.3754 (13)–0.3768 (11)	0.1861 (7)–0.1871 (6)	0.4570 (12)–0.4589 (18)	0.9 (2)–1.3 (2)
	(*a*)	0.3796 (2)	0.18212 (7)	0.4588 (2)	2.860 (4)
	(*b*)	0.3778 (3)	0.1820 (1)	0.4588 (2)	1.90 (3)

	Ca—O1	Ca—O2	Ca—O2^{ii}	Ca—O*W*	S—O1	S—O2	O1—S—O1^{i}	O1—S—O2	O1—S—O2^{i}	O2—S—O2^{i}
1000 s	2.563 (17)	2.535 (17)	2.393 (18)	2.428 (14)	1.465 (16)	1.481 (18)	110.8 (13)	106.0 (8)	112.5 (8)	109.2 (15)
2000 s	2.576 (13)	2.542 (13)	2.379 (13)	2.429 (10)	1.461 (12)	1.486 (14)	109.8 (8)	106.8 (6)	112.1 (6)	109.4 (11)
3000 s	2.576 (12)	2.542 (12)	2.376 (12)	2.423 (10)	1.469 (11)	1.482 (12)	109.8 (8)	107.0 (5)	111.7 (6)	109.7 (10)
4000 s	2.578 (11)	2.529 (11)	2.385 (11)	2.427 (9)	1.469 (10)	1.480 (11)	108.9 (8)	106.4 (5)	112.3 (5)	110.6 (9)
5000 s	2.577 (11)	2.526 (11)	2.384 (11)	2.426 (8)	1.469 (9)	1.482 (11)	108.6 (7)	106.3 (5)	112.6 (5)	110.5 (9)
10000 s	2.577 (9)	2.512 (9)	2.395 (10)	2.429 (8)	1.462 (9)	1.475 (9)	108.5 (7)	105.8 (4)	112.5 (4)	111.7 (8)
20000 s	2.575 (9)	2.520 (9)	2.390 (9)	2.423 (7)	1.465 (8)	1.477 (8)	108.9 (6)	106.1 (4)	112.2 (4)	111.5 (7)
(*a*)	2.546 (1)	2.552 (1)	2.366 (1)	2.374 (1)	1.474 (1)	1.471 (1)	111.1 (1)	106.29 (4)	111.09 (4)	111.0 (1)
(*b*)	2.528 (2)	2.544 (2)	2.378 (1)	2.380 (1)	1.457 (1)	1.461 (1)	111.5 (1)	105.5 (1)	111.7 (1)	111.0 (1)

Symmetry codes: (i) $-x, y, \frac{1}{2} - z$; (ii) $-x, -y, -z$.

The refinement of the data of the nanocrystalline TiO_2 polymorph mixture indicates a satisfactory agreement between the refined [rutile 18.0 (4) wt%, anatase 82.0 (3) wt%] and nominal weight fractions. The *z* coordinate of O of anatase is within 1.5σ of the value reported from single-crystal analysis (Horn *et al.*, 1972), while the displacement parameters are comparable. Cell parameters are also reasonably close to reference data. The refined texture index *J* of anatase, close to one, is consistent with the spherical morphology of the crystallites (Degussa-Hüls technical report 1-1176-0).

Gypsum represents a more challenging test for this instrumental configuration. As can be seen from Table 4, meaningful results have been obtained for this material with collection times as short as 1000 s, despite the relatively large standard deviations of the bond distances and angles. In fact, bond distances are within 1.5σ and angles within 1σ of both neutron (Pedersen & Semmingsen, 1982) and X-ray (Cole & Lancucki, 1974) reference single-crystal data. The larger discrepancy on bond lengths is caused by the Ca—O*W* bond distance, which has been found to be *ca* 0.04 Å systematically larger than the single-crystal value. This may be attributed to the distortion and, corresponding, the displacement of the centre of gravity of the electronic density of O*W* because of the contribution of the two bonded hydrogen atoms. For a counting time of 2000 s, the corresponding standard deviations are reduced to 75%, with only marginal further reduction with increasing collection time. This may be considered as a particularly satisfactory result because it was obtained *via* a completely unrestrained refinement and with a data set that is affected by significant preferred orientation.

5. Conclusions

According to our results, the feasibility to refine relatively simple structures using laboratory EDXD data is confirmed. The results we obtained are further promising because the instrument we used, at present, is not optimized for analysis of crystalline samples as it lacks Soller slits. Although the EDXD technique is ideally suited for synchrotron sources, as it takes full advantage of the properties of this X-ray source, laboratory instruments have the advantage of greater availability. Moreover, whenever long experiments are involved, as in the case of the real-time study of slow time-dependent phenomena, the emission stability of sealed tubes surpasses that of the storage rings. As a final advantage, the relative simplicity of the corrections to be applied to the raw data is significant.

References

Ballirano, P., Caminiti, R., Ercolani, C., Maras, A. & Orrù, M. A. (1998). *J. Am. Chem. Soc.* **120**, 12798–12807.
Buras, B., Gerward, L., Glazer, A. M., Hidaka, M. & Staun Olsen, J. (1979). *J. Appl. Cryst.* **12**, 531–536.

Caminiti, R., Carbone, M., Panero, S. & Sadun, C. (1999). *J. Phys. Chem. B*, **103**, 10348–10355.
Caminiti, R., Gleria, M., Lipkowitz, K. B., Lombardo, G. M. & Pappalardo, G. C. (1997). *J. Am. Chem. Soc.* **119**, 2196–2204.
Caminiti, R. & Rossi Albertini, V. (1999). *Int. Rev. Phys. Chem.* **18**, 263–299.
Caminiti, R., Sadun, C., Bionducci, M., Buffa, F., Ennas, G., Licheri, G. & Musinu, A. (1997). *Gazz. Chim. Ital.* **127**, 59–62.
Caminiti, R., Sadun, C., Rossi, V., Cilloco, F. & Felici, R. (1991). *XXV National Congress of Physical Chemistry*, Cagliari, Italy, 17–21 June 1991; Italian Patent Appl. 01261484, 23 June 1993.
Cline, J. P. & Cheary, R. W. (1998). *The Design, Alignment, Calibration and Performance Characteristics of the Conventional Laboratoty Diffractometer.* Workshop notes from the 45th and 47th Denver X-ray conference.
Cole, W. F. & Lancucki, C. J. (1974). *Acta Cryst.* B**30**, 921–929.
Drever, J. I. & Fitgerald, R. W. (1970). *Mater. Res. Bull.* **5**, 101–107.
Eisenreich, N. & Engel, W. (1983). *J. Appl. Cryst.* **16**, 259–263.
Ferrel, R. F. Jr (1971). *Am. Mineral.* **56**, 1822–1831.
Finger, L. W., Cox, D. E. & Jephcoat, A. P. (1994). *J. Appl. Cryst.* **27**, 892–900.
Frost, D. J. & Fei, Y. (1999). *Phys. Chem. Miner.* **26**, 415–418.
Giessen, B. C. & Gordon, G. E. (1968). *Science*, **159**, 973–975.
Glazer, A. M., Hidaka, M. & Bordas, J. (1978). *J. Appl. Cryst.* **11**, 165–172.
Grevel, K.-D., Nowlan, E. U., Fasshauer, D. W. & Burchard, M. (2000). *Am. Mineral.* **85**, 206–216.
Hill, R. J. & Madsen, I. C. (1986). *J. Appl. Cryst.* **19**, 10–18.
Horn, M., Schwerdtfeger, C. F. & Meagher, E. P. (1972). *Zeit. Krist.* **136**, 273–281.
Laine, E., Lähteenmäki, T. & Hämäläinen, M. (1974). *J. Phys. E*, **7**, 951–952.
Larson, A. C. & Von Dreele, R. B. (1985). *GSAS: General Structure Analysis System.* LAUR 86-748, Los Alamos National Laboratory, New Mexico, USA.
Lewis, J., Schwarzenbach, D. & Flack, H. D. (1982). *Acta Cryst.* A**38**, 733–739.
Morishima, H., Ohtani, E., Kato, T., Kubo, T., Suzuki, A., Kikegawa, T. & Shimomura, O. (1999). *Phys. Chem. Miner.* **27**, 3–10.
Nakajima, T., Fukamachi, T., Terasaki, O. & Hosoya, S. (1976). *J. Appl. Cryst.* **9**, 286–290.
Nuding, W., Hinze, E. & Will, G. (1980). *J. Appl. Cryst.* **13**, 46–49.
Oetzel, M. & Heger, G. (1999). *J. Appl. Cryst.* **32**, 799–807.
Otto, J. W. (1997). *J. Appl. Cryst.* **30**, 1008–1015.
Pedersen, B. F. & Semmingsen, D. (1982). *Acta Cryst.* B**38**, 1074–1077.
Rietveld, H. M. (1969). *J. Appl. Cryst.* **2**, 65–71.
Rossi Albertini, V., Bencivenni, L., Caminiti, R., Cilloco, F. & Sadun, C. (1996). *J. Macromol. Sci. Phys. B*, **35**, 199–213.
Rossi Albertini, V., Caminiti, R., Cilloco, F., Croce, F. & Sadun, C. (1997). *J. Macromol. Sci. Phys. B*, **36**, 221–232.
Shintani, H., Sato, S. & Saito, Y. (1975). *Acta Cryst.* B**31**, 1981–1982.
Sugiyama, K., Shinkai, T. & Waseda, Y. (1998). *High Temp. Mater. Proc.* **17**, 155–161.
Thompson, P., Cox, D. E. & Hastings, J. B. (1987). *J. Appl. Cryst.* **20**, 79–83.
Uno, R. & Ishigaki, J. (1984). *J. Appl. Cryst.* **17**, 154–158.
Von Dreele, R. B. (1997). *J. Appl. Cryst.* **30**, 517–525.
Will, G., Parrish, W. & Huang, T. C. (1983). *J. Appl. Cryst.* **16**, 611–622.
Wilson, A. J. C. (1973). *J. Appl. Cryst.* **6**, 230–237.
Yamanaka, T. & Ogata, K. (1991). *J. Appl. Cryst.* **24**, 111–118.
Young, R. A. (1993). *The Rietveld Method*, pp. 1–38. Oxford University Press.
Zang, J. & Guyot, F. (1999). *Phys. Chem. Miner.* **26**, 419–426.